


 Cite this: *RSC Adv.*, 2020, 10, 9093

Effect of NH₃ and HCOOH on the H₂O₂ + HO → HO₂ + H₂O reaction in the troposphere: competition between the one-step and stepwise mechanisms†

 Tianlei Zhang,[†] Mingjie Wen,[‡] Zhaopeng Zeng,[‡] Yousong Lu,[‡] Yan Wang,[‡] Wei Wang,[†] Xianzhao Shao,^{*a} Zhiyin Wang^a and Lily Makroni^{*b}

The H₂O₂ + HO → HO₂ + H₂O reaction is an important reservoir for both radicals of HO and HO₂ catalyzing the destruction of O₃. Here, this reaction assisted by NH₃ and HCOOH catalysts was explored using the CCSD(T)-F12a/cc-pVDZ-F12//M06-2X/aug-cc-pVTZ method and canonical variational transition state theory with small curvature tunneling. Two possible sets of mechanisms, (i) one-step routes and (ii) stepwise processes, are possible. Our results show that in the presence of both NH₃ and HCOOH catalysts under relevant atmospheric temperature, mechanism (i) is favored both energetically and kinetically than the corresponding mechanism (ii). At 298 K, the relative rate for mechanism (i) in the presence of NH₃ (10, 2900 ppbv) and HCOOH (10 ppbv) is respectively 3–5 and 2–4 orders of magnitude lower than that of the water-catalyzed reaction. This is due to a comparatively lower concentration of NH₃ and HCOOH than H₂O which indicates the positive water effect under atmospheric conditions. Although NH₃ and HCOOH catalysts play a negligible role in the reservoir for both radicals of HO and HO₂ catalyzing the destruction of O₃, the current study provides a comprehensive example of how acidic and basic catalysts assisted the gas-phase reactions.

 Received 2nd January 2020
 Accepted 13th February 2020

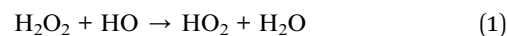
DOI: 10.1039/d0ra00024h

rsc.li/rsc-advances

1. Introduction

Hydrogen peroxide (H₂O₂) is of great importance not only because it is involved in various biological and atmospheric processes,¹ but it's also one of the major sources of hydroxyl (HO) and hydroperoxyl (HO₂) radicals which play an important role in combustions and atmospheric chemical processes.¹ Hydroxyl radical (HO) plays an important role in maintaining the balance of atmospheric composition and forming reactive peroxides.^{2,3} Also, from the standpoint of degradation ability,^{4,5} HO radicals can react with one ozone molecule to produce molecular oxygen and the HO₂ radicals in the upper atmosphere. As an important reaction in HO_x chemistry, the H₂O₂ +

HO reaction shown in eqn (1) can determine the consumption of HO radicals in HO_x chain reactions. Meanwhile, this reaction is also an important reservoir^{5,6} for both radicals of HO and HO₂ catalyzing the destruction of ozone (O₃).



It is obvious from previous reports that the H₂O₂ + HO reaction has been extensively studied both experimentally^{7–12} and theoretically.^{10,13–15} In terms of experiments, for the gas-phase reaction of H₂O₂ + HO, Vakhtin *et al.*¹⁶ obtained its rate coefficient (1.78 ± 0.19) × 10^{−12} cm³ per molecule per s at 296 K through the laser-induced resonance fluorescence technology. Similar to the report of Vakhtin *et al.*,¹⁶ NASA/JPL¹⁷ evaluation suggested the rate coefficient for the H₂O₂ + HO reaction between 200 and 300 K was 1.8 × 10^{−12} cm³ per molecule per s. In addition, the results obtained by the experimental group^{18,19} revealed that the rate coefficients for the H₂O₂ + HO reaction have positive temperature dependence within different temperature ranges. From the theoretical point of view, Francisco's group²⁰ has studied the mechanism of H₂O₂ + HO reaction at the CCSD(T)/CBS//MP2/aug-cc-pVDZ level, and their calculated rate coefficient was 1.56 × 10^{−12} cm³ per molecule per s at 298 K, which was in good agreement with the experimental results reported by Vaghjani and coworkers.¹⁰ Then,

^aShaanxi Key Laboratory of Catalysis, School of Chemical & Environment Science, Shaanxi University of Technology, Hanzhong, Shaanxi 723001, P. R. China. E-mail: ztianlei88@163.com; xianzhao@snut.edu.cn; Fax: +86-916-2641083; Tel: +86-916-2641083

^bKey Laboratory for Macromolecular Science of Shaanxi Province, School of Chemistry & Chemical Engineering, Shaanxi Normal University, Xi'an, Shaanxi 710062, P. R. China. E-mail: lilymakroni@gmail.com

^cShanghai Key Laboratory of Molecular Catalysis and Innovative Materials, Fudan University, Shanghai 200433, P. R. China

† Electronic supplementary information (ESI) available. See DOI: 10.1039/d0ra00024h

‡ Mingjie Wen, Zhaopeng Zeng, Yousong Lu and Yan Wang are contributed equally to this work.



a water-assisted $\text{H}_2\text{O}_2 + \text{HO}$ reaction has been reported by Francisco's group. Their calculations show that the rate coefficient for the $\text{H}_2\text{O}_2 + \text{HO}$ reaction with H_2O was $4.09 \times 10^{-12} \text{ cm}^3$ per molecule per s at 298 K, which was 2.6 times larger than the value of the unassisted reaction. Subsequently, the reactions of $\text{H}_2\text{O}_2 \cdots (\text{H}_2\text{O})_n$ ($n = 1-3$) + HO and $\text{H}_2\text{O}_2 + \text{HO} \cdots (\text{H}_2\text{O})_n$ ($n = 1-3$) have been investigated by our group,²¹ where the catalytic effect of $(\text{H}_2\text{O})_n$ ($n = 1-3$) is mainly taken from the contribution of H_2O , and in H_2O -assisted reaction, one-step process occurring through cage-like hydrogen bonding network complex and the transition state is kinetically favorable. However, this effort has focused only on the process of $\text{H}_2\text{O}_2 + \text{HO}$ reaction without and with water. As far as we know, the effect of NH_3 and HCOOH on $\text{H}_2\text{O}_2 + \text{HO} \rightarrow \text{HO}_2 + \text{H}_2\text{O}$ reaction has not been elucidated in the literature yet.

As the most abundant of all alkaline gases, the concentration of NH_3 was found to be 10 ppm in dairy farms and 30 ppb in a polluted ambient atmosphere.²²⁻²⁵ Meanwhile, NH_3 has similar efficiency as H_2O in catalyzing many hydrogen abstraction reactions.²⁶⁻³⁰ Based on the fact that the possibility of the NH_3 -catalytic effect on the $\text{H}_2\text{O}_2 + \text{HO} \rightarrow \text{HO}_2 + \text{H}_2\text{O}$ reaction has been investigated theoretically in this work. Also, owing to the significant abundance of HCOOH in the atmosphere, HCOOH can also be an effective catalyst like H_2O and NH_3 . It has been proved in previous investigations that HCOOH can decrease the energy significantly for several atmospheric hydrogen abstraction reactions.³¹⁻³⁷ Thus, it is also necessary to study the possible catalytic effect of HCOOH on the $\text{H}_2\text{O}_2 + \text{HO}$ reaction.

In the present work, the effect of NH_3 and HCOOH on the $\text{H}_2\text{O}_2 + \text{HO} \rightarrow \text{HO}_2 + \text{H}_2\text{O}$ reaction has been investigated from both energetic and kinetic aspects, which was organized in two ways. Firstly, the roles of NH_3 and HCOOH in the $\text{H}_2\text{O}_2 + \text{HO} \rightarrow \text{HO}_2 + \text{H}_2\text{O}$ reaction have been studied by both stepwise mechanism and one-step process. Then, the relative impacts of NH_3 and HCOOH and their competition with H_2O have been investigated by considering the dependence of rate coefficient on temperature and catalyst concentrations. Through our research, we expect to provide significant theoretical guidance for further revealing of the $\text{H}_2\text{O}_2 + \text{HO} \rightarrow \text{HO}_2 + \text{H}_2\text{O}$ reaction assisted by acidic, neutral and basic catalysts in the actual atmospheric environment.

2. Computational methods

2.1 Electronic structure calculation

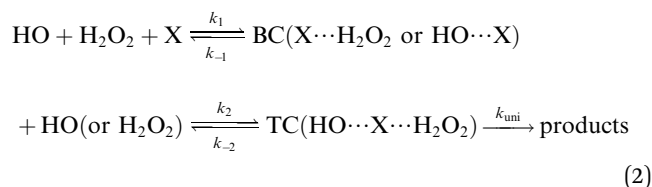
The electronic structure calculations have been carried out by the Gaussian 09 program.³⁸ Geometries of all the species including reactants, pre-reactive complexes, transition states, post-reactive complexes, and products were optimized at the M06-2X/aug-cc-pVTZ level. The corresponding frequencies of the optimized geometries were computed at the same level to prove the characteristics of the transition states with one imaginary frequency and the stationary points possess all real frequencies. The minimum energy paths (MEPs) were obtained by intrinsic reaction coordinate (IRC)³⁹⁻⁴¹ calculations at the same level which confirms TSs, reactants, and products. IRC

calculations also confirmed the presence of pre- and post-reactive complexes at the entry and exit site of reaction path.

To improve the accuracy of the energetics, using M06-2X/aug-cc-pVTZ optimized geometries, single-point energy was calculated using ORCA⁴² at the CCSD(T)-F12a/cc-pVDZ-F12 level,⁴³⁻⁴⁵ and the scaled ZPEs were added to them. The scaling factor employed to adjust the ZPEs was 0.9490.⁴⁶ The reliability of CCSD(T)-F12a/cc-pVDZ-F12 method was further tested by the single point energies of $\text{H}_2\text{O}_2 + \text{HO} \rightarrow \text{HO}_2 + \text{H}_2\text{O}$ reaction at the W3X-L and W2X⁴⁷ using MRCC^{48,49} program packages. It is noted that quantitative barrier heights^{47,50-53} for complex atmospheric reactions can be obtained using W3X-L, where the accuracy of W2X and W3X-L can respectively reach for the all-electron scalar-relativistic CCSD(T)/CBS and CCSD(Q)/CBS. Here, the calculated results showed that the unsigned error of CCSD(T)-F12a/cc-pVDZ-F12 is less than $0.5 \text{ kcal mol}^{-1}$ (Table S1†), when compared with W3X-L results. Therefore, the affordable CCSD(T)-F12a/cc-pVDZ-F12 method is chosen to do single point energy calculations for the $\text{H}_2\text{O}_2 + \text{HO} \rightarrow \text{HO}_2 + \text{H}_2\text{O}$ reaction assisted by NH_3 and HCOOH .

2.2 Chemical kinetics calculations

$\text{H}_2\text{O}_2 + \text{HO} \rightarrow \text{HO}_2 + \text{H}_2\text{O}$ reaction assisted by catalyst X (X = NH_3 and HCOOH) can be regarded as a sequential bimolecular reaction shown in eqn (2).



In eqn (2), the dimer $\text{H}_2\text{O}_2 \cdots \text{HO}$ is assumed to be less important than $\text{H}_2\text{O}_2 \cdots \text{X}$ and $\text{HO} \cdots \text{X}$, due to the small concentration of H_2O_2 and HO radicals. So, the sequential bimolecular route would first occur through the formation of a bimolecular complex BC ($\text{X} \cdots \text{H}_2\text{O}_2$ or $\text{HO} \cdots \text{X}$), and then bimolecular complex combines with the other reactant (HO or H_2O_2) to form the trimolecular complex TC ($\text{HO} \cdots \text{X} \cdots \text{H}_2\text{O}_2$). Subsequently, the trimolecular complex undergoes a unimolecular reaction *via* the corresponding TS to form the products. Assuming a steady-state approximation, trimolecular complex TC is in equilibrium with bimolecular complex BC and reactant (H_2O_2 or HO), the bimolecular rate coefficient (k_b) for the reaction between BC and reactant (H_2O_2 or HO) can be written as eqn (3) and calculated by employing Polyrate 8.2 program⁵⁴ coupled with the steady-state approximation.

$$k_b = \frac{k_2}{k_{-2} + k_{\text{uni}}} k_{\text{uni}} \quad (3)$$

Here assuming k_{-2} is much larger than k_{uni} , k_b of eqn (3) can be simplified as eqn (4).

$$k_b = K_{\text{eq2}} \times k_{\text{uni}} \quad (4)$$

This kinetic model is reasonably correct at the high-pressure limit. In eqn (4), the equilibrium constant K_{eq2} can be written in



eqn (5), while the rate coefficient constant (k_{uni}) from trimolecular complex to the products can be minimized by varying the transition state dividing surface along the reaction coordinate to get the CVT rate coefficients given by eqn (6) and (7):^{55–58}

$$K_{\text{eq2}}(T) = \sigma \frac{Q_{\text{TC}}}{Q_{\text{R}} Q_{\text{BC}}} \exp\left(\frac{E_{\text{R}} + E_{\text{BC}} - E_{\text{TC}}}{RT}\right) \quad (5)$$

$$k^{\text{GT}}(T, s) = \Gamma L^{\ddagger} \times \frac{k_{\text{B}} T}{h} \frac{Q_{\text{TS}}^{\ddagger}(T, s)}{Q_{\text{TC}}(T)} \exp\left(-\frac{V_{\text{MEP}}(s)}{k_{\text{B}} T}\right) \quad (6)$$

$$k^{\text{CVT}}(T) = \min_s k^{\text{GT}}(T, (s)) = k^{\text{GT}}[T, s^{\text{CVT}}(T)] \quad (7)$$

where Q_{TC} , Q_{BC} and Q_{R} in eqn (5) is respectively the total partition function of the trimolecular complex TC, bimolecular complex BC and reactant (HO or H_2O_2); E_{TC} , E_{BC} and E_{R} is respectively the energy of trimolecular complex TC, bimolecular complex BC and reactant (HO or H_2O_2). $k^{\text{GT}}(T, s)$ in eqn (6) and $k^{\text{CVT}}(T)$ in eqn (7) is respectively the rate coefficient of generalized and canonical variational transition state theory. Γ is the small curvature tunneling (SCT)^{59,60} correction, L^{\ddagger} is the reaction path degeneracy, h is the Planck's constant, k_{B} is the Boltzmann constant, $V_{\text{MEP}}(s)$ is the classical barrier height and Q_{TS}^{\ddagger} is the total partition functions for the transition state. It should be noted that K_{eq2} calculated here has been successfully performed in calculating the complexes^{61–65} of $\text{H}_2\text{O} \cdots \text{VOC}$, $\text{H}_2\text{O} \cdots \text{HCHO}$, $\text{H}_2\text{O} \cdots \text{CH}_3\text{COCH}_3$, $\text{H}_2\text{O} \cdots \text{CH}_2\text{NH}$, $\text{H}_2\text{O} \cdots \text{HO}_2$, $\text{H}_2\text{O} \cdots \text{SO}_2$, and $\text{H}_2\text{O} \cdots \text{NO}_2$. In this work, we do not consider the effects of partial pressure on the formation of these complexes because there are no experimental data to show that the equilibrium constants of these complexes are determined by pressure.

The equilibrium constant for the formation of the bimolecular complex (K_{eq1}) can also be calculated using corresponding partition functions and energies (obtained from electronic structure calculations) as eqn (8)

$$K_{\text{eq1}}(T) = \sigma \frac{Q_{\text{BC}}}{Q_{\text{R}} Q_{\text{X}}} \exp\left(\frac{E_{\text{R}} + E_{\text{X}} - E_{\text{BC}}}{RT}\right) \quad (8)$$

where Q_{BC} and Q_{R} are the total partition functions of the bimolecular complex and reactants, respectively; E_{BC} and E_{R} are the energies of bimolecular complex and reactants, respectively. From the above, the rate (ν) of the sequential bimolecular reaction can be written as:

$$\nu = K_{\text{eq1}} \times K_{\text{eq2}} \times k_{\text{uni}} \times [\text{X}] \times [\text{HO}] \times [\text{H}_2\text{O}_2] \quad (9)$$

Here, ν is considered as a measure of the relative efficiencies of the different catalysts under atmospheric conditions.

3. Results and discussions

3.1 Reactants

In the presence of catalyst X, the $\text{H}_2\text{O}_2 + \text{HO} + \text{X}$ reaction going through a termolecular reaction has a much lower probability than the sequential bimolecular reaction. In this work, the sequential bimolecular reaction is that, initially, the $\text{H}_2\text{O}_2 + \text{HO} + \text{X}$ reaction goes through a two-body complex between catalyst

X and one of the two reactants (H_2O_2 or HO) and then the two-body complex will react with the other reactant. It should be noted that, because of the small concentration of H_2O_2 and HO radicals, the concentration of dimer $\text{H}_2\text{O}_2 \cdots \text{HO}$ is much lower as compared to the dimers of $\text{H}_2\text{O}_2 \cdots \text{X}$ and $\text{HO} \cdots \text{X}$. Thus, $\text{H}_2\text{O}_2 \cdots \text{HO}$ complex can be neglected and it is not taken into account here. Such investigations have been studied in similar investigations,^{52,66–70} where the dimer between the two reactants has not been involved in X assisted reactions. Above step is followed since it is very necessary to first identify the stable binary complexes of $\text{H}_2\text{O}_2 \cdots \text{X}$ and $\text{HO} \cdots \text{X}$. To achieve this aim, we performed a stable global minimum searching of geometrical configurations using Tsinghua Global Minimum (TGMin) program^{71,72} to search out variety geometrical configurations of $\text{H}_2\text{O}_2 \cdots \text{X}$ and $\text{HO} \cdots \text{X}$ complexes firstly. Secondly initial structures obtained for these binary complexes were selected for geometry optimization using the M06-2X/6-31+G(d,p) level. Then, the structures within 5.0 kcal mol⁻¹ of the global minimum were re-optimized by M06-2X/aug-cc-pVTZ level. The optimized structures for the most stable $\text{H}_2\text{O}_2 \cdots \text{X}$ and $\text{HO} \cdots \text{X}$ complexes have been shown in Fig. 1. As displayed in Fig. 1, the stable binary $\text{H}_2\text{O}_2 \cdots \text{NH}_3$ complex shows a five-membered ring with two hydrogen bonds ($\text{H4} \cdots \text{N}$, 1.85 Å; $\text{H1} \cdots \text{O2}$, 2.67 Å) involved. Its stabilization energy is 6.6 kcal mol⁻¹ relative to the separate reactants of H_2O_2 and NH_3 , and is respectively stabilized by 1.1 and 6.6 kcal mol⁻¹ than the other two binary complexes of $\text{HO} \cdots \text{NH}_3$ and $\text{NH}_3 \cdots \text{HO}$. Binary complexes of $\text{H}_2\text{O}_2 \cdots \text{HCOOH}$ and $\text{HO} \cdots \text{HCOOH}$ were formed with stabilization energies of 10.1 and 4.9 kcal mol⁻¹, respectively. The energy difference between these two complexes can be explained in terms of ring size formed within their structures. The former complex is formed with a seven-membered ring structure, while the latter complex forms a six-membered ring structure.

3.2 Mechanism and kinetic for NH_3 -assisted reaction

Depending on the type of the binary complex discussed above, three different binary mechanisms, labelled as $\text{H}_2\text{O}_2 \cdots \text{NH}_3 + \text{HO}$, $\text{HO} \cdots \text{NH}_3 + \text{H}_2\text{O}_2$, and $\text{NH}_3 \cdots \text{HO} + \text{H}_2\text{O}_2$, were obtained (as illustrated in Fig. 2). Among the three NH_3 assisted $\text{H}_2\text{O}_2 + \text{HO} \rightarrow \text{HO}_2 + \text{H}_2\text{O}$ reactions, one proceeds through both one-step and stepwise mechanisms and the other two occur-only through a one-step mechanism. The relative energies to the separate reactants in the presence of NH_3 are given in Table S5.†

As for Channel R_AM1, the reaction starting with $\text{H}_2\text{O}_2 \cdots \text{NH}_3 + \text{HO}$ reactants leads to a termolecular hydrogen bond complex IM_AM1 with a binding energy of 9.5 kcal mol⁻¹ relatives to the separate $\text{H}_2\text{O}_2 \cdots \text{NH}_3 + \text{HO}$ reactants. Because of the geometry, additional two hydrogen bonds ($\text{N} \cdots \text{H5}$, 1.99 Å; $\text{O3} \cdots \text{H1}$, 2.14 Å) were formed in complex IM_AM1 as compared to $\text{H}_2\text{O}_2 \cdots \text{NH}_3$ complex. This leads to complex IM_WM1 shows a quasi-planar cage-like hydrogen bonding network structure. Starting from complex IM_AM1, Channel R_AM1 proceeds through the transition state TS_AM1 where the O atom of HO radical extracts one H atom of H_2O_2 moiety in $\text{H}_2\text{O}_2 \cdots \text{NH}_3$ complex. As illustrated in Fig. 2(a), TS_AM1 has a computed



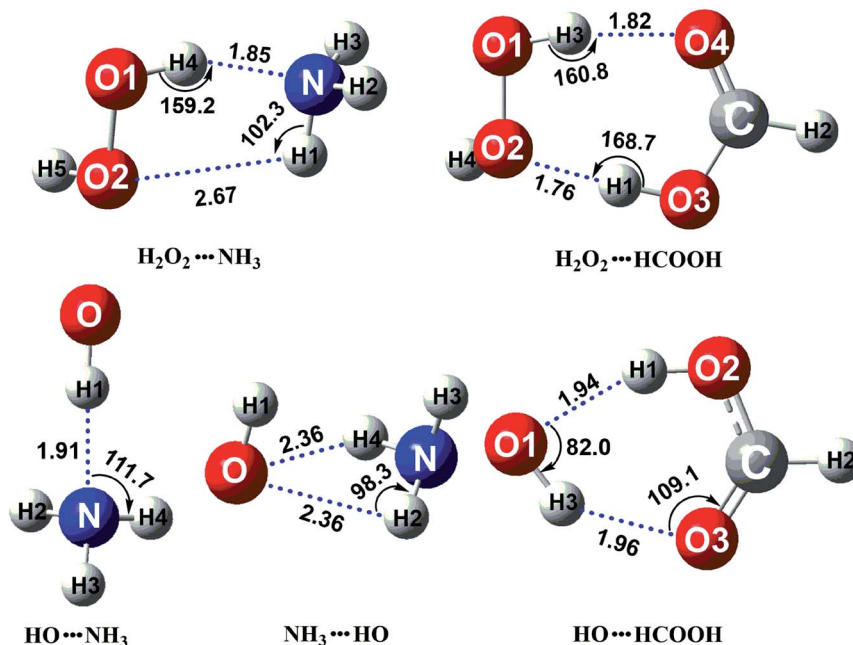


Fig. 1 The optimized structures for the most stable complex of H_2O_2 (or HO) with catalyst X ($X = \text{NH}_3$ and HCOOH) at the CCSD(T)-F12a/cc-pVDZ-F12//M06-2X/aug-cc-pVTZ level.

barrier of $9.2 \text{ kcal mol}^{-1}$ relative to complex IM_AM1. This barrier height is much lower than that for $\text{H}_2\text{O}_2 + \text{HO} \rightarrow \text{HO}_2 + \text{H}_2\text{O}$ reaction without catalyst X, which has an energy barrier of $14.1 \text{ kcal mol}^{-1}$ as compared to corresponding pre-reactive complex IM1 (Table S5[†]). Similarity, compared with the reaction without X, the computed free energy barrier (ΔG , 298 K) of the transition state TS_AM1 to the complex IM_AM1 is reduced to $9.6 \text{ kcal mol}^{-1}$ from $14.1 \text{ kcal mol}^{-1}$. Differently from complex IM_AM1 and transition state TS_AM1, post-reactive complex IMF_AM1 shows a planar structure with its stabilization energy of $42.5 \text{ kcal mol}^{-1}$ relative to $\text{H}_2\text{O}_2 \cdots \text{NH}_3 + \text{HO}$ reactants.

As for Channel R_AM2, when NH_3 has introduced into the $\text{H}_2\text{O}_2 + \text{HO} \rightarrow \text{HO}_2 + \text{H}_2\text{O}$ reaction, two kinds of entrance channels, $\text{H}_2\text{O}_2 \cdots \text{NH}_3 + \text{HO}$ (Path R_AM2a) and $\text{HO} \cdots \text{NH}_3 + \text{H}_2\text{O}_2$ (Path R_AM2b), have been displayed in Fig. 2(b). When binary complex $\text{H}_2\text{O}_2 \cdots \text{NH}_3$ and HO play as reactants, the reaction occurs in stepwise route, which is similar to H_2O catalyzed reactions^{21,28,62,73,74} of $\text{HO}_2 + \text{HO}$, $\text{HO}_2 + \text{HS}$, $\text{H}_2\text{O}_2 + \text{HO}$, $\text{HO}_2 + \text{Cl}$, and $\text{HO}_2 + \text{NH}_2$, as well as NH_3 -catalyzed $\text{HO}_2 + \text{Cl}$ reaction.²⁸ The first step begins with pre-reactive complex IM_AM2, which transforms into seven-membered ring complex IM_AM3 through transition state TS_AM2 by a ring enlargement. It is noted that complex IM_AM3 has a binding energy of $11.8 \text{ kcal mol}^{-1}$, larger by $5.3 \text{ kcal mol}^{-1}$ that of complex IM_AM2. At the same time, the barrier height of the ring enlargement is only $2.6 \text{ kcal mol}^{-1}$, revealing that this elementary step can occur easily both thermodynamically and kinetically. In the second step, the IM_AM3 complex undergoes a direct hydrogen abstraction by the O atom of HO moiety abstracting one H atom of H_2O_2 moiety. This elementary step overcomes a barrier height of $4.4 \text{ kcal mol}^{-1}$, which is higher by

$1.8 \text{ kcal mol}^{-1}$ than the corresponding barrier height for the step of ring enlargement. This reveals that the second step is the rate-determining step. When $\text{HO} \cdots \text{NH}_3$ and H_2O_2 act as reactants, the reaction occurs in one elementary step, which is similar to the $\text{H}_2\text{O}_2 + \text{HO} \rightarrow \text{HO}_2 + \text{H}_2\text{O}$ reaction in the absence of a catalyst. Starting from $\text{HO} \cdots \text{NH}_3 + \text{H}_2\text{O}_2$ reactants, Path R_AM2b starts with pre-reactive complex IM_AM3 and proceeds through the transition state TS_AM3 to from the post-reactive complex IMF_AM3, which has been discussed above. To check the competition between $\text{H}_2\text{O}_2 \cdots \text{NH}_3 + \text{HO}$ and $\text{HO} \cdots \text{NH}_3 + \text{H}_2\text{O}_2$ in Channel R_AM2, the rate *via* the routes of $\text{H}_2\text{O}_2 \cdots \text{NH}_3 + \text{HO}$ (Path R_AM2a) and $\text{HO} \cdots \text{NH}_3 + \text{H}_2\text{O}_2$ (Path R_AM2b) is respectively given in eqn (10) and (11).

$$v_{\text{R_AM2a}} = \frac{d[\text{HO}_2]}{dt} = K_{\text{eq1a}} \times k_{\text{R_AM2a}} \times [\text{H}_2\text{O}_2] \times [\text{NH}_3] \times [\text{HO}] \quad (10)$$

$$v_{\text{R_AM2b}} = \frac{d[\text{HO}_2]}{dt} = K_{\text{eq1b}} \times k_{\text{R_AM2b}} \times [\text{H}_2\text{O}_2] \times [\text{NH}_3] \times [\text{HO}] \quad (11)$$

where K_{eq1a} and K_{eq1b} respectively denote the equilibrium constant for the formation of $\text{H}_2\text{O}_2 \cdots \text{NH}_3$ and $\text{HO} \cdots \text{NH}_3$; $k_{\text{R_AM2a}}$ and $k_{\text{R_AM2b}}$ respectively denote the bimolecular rate constant of Path R_AM2a and Path R_AM2b. The calculated rate ratio for $v_{\text{R_AM2a}}/v_{\text{R_AM2b}}$ reveals that the entrance of $\text{HO} \cdots \text{NH}_3$ and H_2O_2 is more important than that of $\text{H}_2\text{O}_2 \cdots \text{NH}_3$ and HO with the ratio of $v_{\text{R_AM2a}}/v_{\text{R_AM2b}}$ is 5.99×10^{-6} to 2.36×10^{-5} between 280 and 320 K (Table 1). As a result, Channel R_AM2 occurs mainly through $\text{HO} \cdots \text{NH}_3 + \text{H}_2\text{O}_2$ reactants. Similarity, the $\text{NH}_3 \cdots \text{HO} + \text{H}_2\text{O}_2$ reaction (Path R_AM3b) only has been taken into account in Channel R_AM3, and the reaction starting



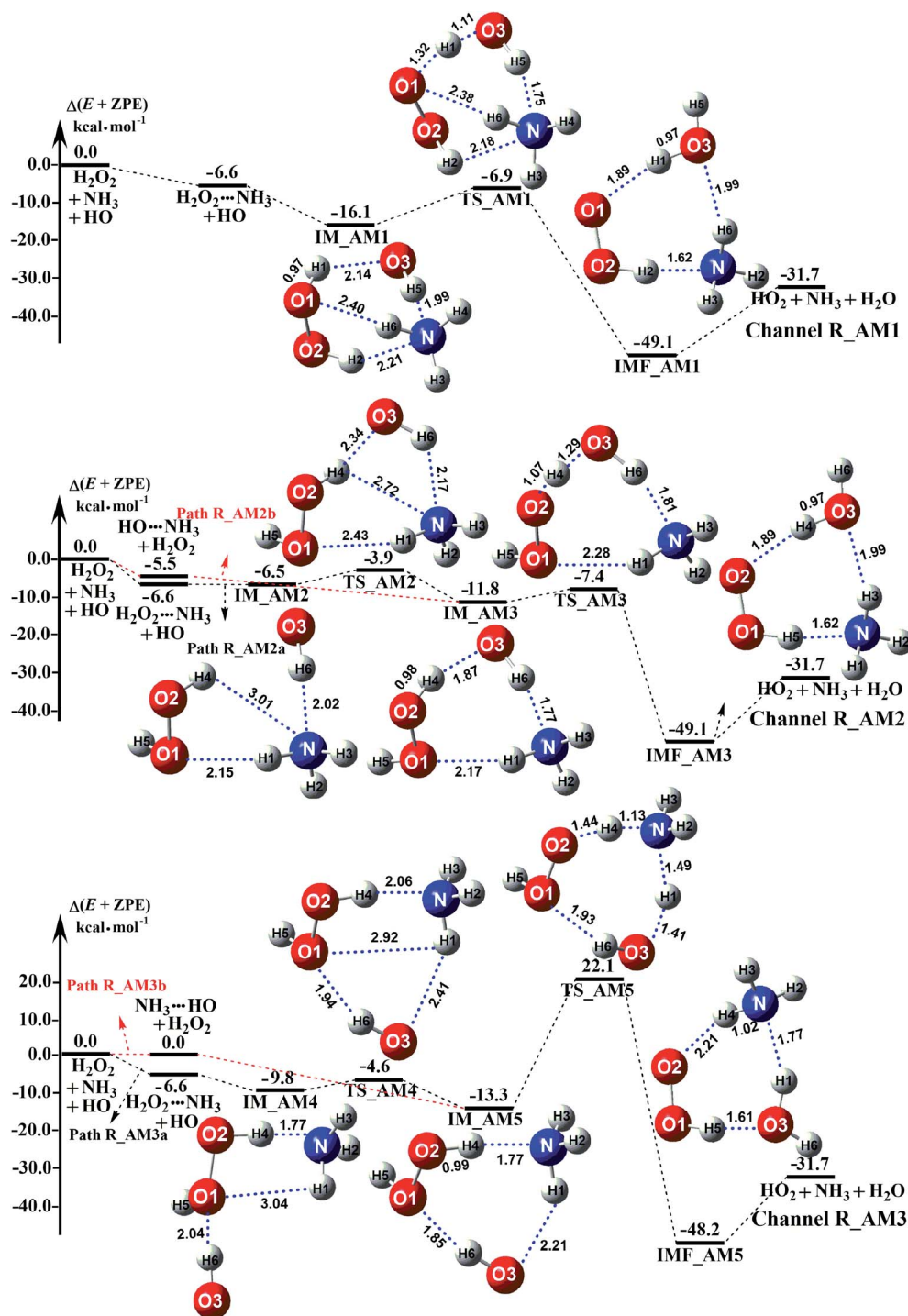


Fig. 2 Schematic potential energy diagrams for NH_3 catalyzed $\text{H}_2\text{O}_2 + \text{HO} \rightarrow \text{HO}_2 + \text{H}_2\text{O}$ reaction at the CCSD(T)-F12a/cc-pVDZ-F12//M06-2X/aug-cc-pVTZ level.

from $\text{H}_2\text{O}_2 \cdots \text{NH}_3 + \text{HO}$ reactants (Path R_AM3a) has been neglected because the ratio of $\nu_{\text{R_AM3a}}/\nu_{\text{R_AM3b}}$ listed in Table 1 is 3.45×10^{-3} to 7.24×10^{-3} between 280 and 320 K.

Regarding Channel R_AM3 starting from $\text{NH}_3 \cdots \text{HO} + \text{H}_2\text{O}_2$ reactants, seven-membered ring complex IM_AM5 proceeded through transition state TS_AM5 to post-reactive complex R_AM2 and R_AM3 is possibly due to that Channel R_AM2 involves a direct hydrogen abstraction, whereas double

that the barrier height of Channel R_AM3 is $31.0 \text{ kcal mol}^{-1}$ higher than the corresponding barrier height value involved in Channel R_AM2, while the computed free energy barrier (ΔG , 298 K) of Channel R_AM3 is higher by $32.9 \text{ kcal mol}^{-1}$ than that of Channel R_AM2. Such energy difference between Channels R_AM2 and R_AM3 is possibly due to that Channel R_AM2 involves a direct hydrogen abstraction, whereas double



Table 1 The bimolecular rate coefficients (cm^3 per molecules per s) and rate ratio for NH_3 catalyzed $\text{H}_2\text{O}_2 + \text{HO} \rightarrow \text{HO}_2 + \text{H}_2\text{O}$ reaction within the temperature range of 280–320 K

T/K	$k_{\text{R_AM1}}$	$k_{\text{R_AM2a}}$	$k_{\text{R_AM2b}}$	$\nu_{\text{R_AM2a}}/\nu_{\text{R_AM2b}}$	$k_{\text{R_AM3a}}$	$k_{\text{R_AM3b}}$	$\nu_{\text{R_AM3a}}/\nu_{\text{R_AM3b}}$	$\nu_{\text{R_AM2b}}/\nu_{\text{R_AM3b}}$	$\nu_{\text{R_AM1}}/\nu_{\text{R_AM2b}}$
280	1.35×10^{-10}	2.06×10^{-16}	5.91×10^{-11}	5.99×10^{-6}	2.49×10^{-34}	3.54×10^{-28}	3.45×10^{-3}	4.75×10^{20}	3.95
290	1.13×10^{-10}	2.54×10^{-16}	4.68×10^{-11}	8.77×10^{-6}	4.98×10^{-34}	3.92×10^{-28}	4.24×10^{-3}	2.46×10^{20}	3.91
298	9.95×10^{-11}	2.98×10^{-16}	3.93×10^{-11}	1.17×10^{-5}	8.84×10^{-34}	4.47×10^{-28}	4.93×10^{-3}	1.42×10^{20}	3.92
300	9.64×10^{-11}	3.09×10^{-16}	3.75×10^{-11}	1.25×10^{-5}	1.02×10^{-33}	4.63×10^{-28}	5.14×10^{-3}	1.24×10^{20}	3.91
310	8.39×10^{-11}	3.70×10^{-16}	3.06×10^{-11}	1.74×10^{-5}	2.14×10^{-33}	5.81×10^{-28}	6.14×10^{-3}	6.09×10^{19}	3.94
320	7.43×10^{-11}	4.38×10^{-16}	2.55×10^{-11}	2.36×10^{-5}	4.58×10^{-33}	7.69×10^{-28}	7.24×10^{-3}	2.93×10^{19}	4.01

hydrogen transfers were involved in Channel R_AM3. This mechanism discrepancy between Channels R_AM2 and R_AM3 is consistent with water-catalyzed $\text{H}_2\text{O}_2 + \text{HO} \rightarrow \text{HO}_2 + \text{H}_2\text{O}$ reaction.²¹ Hence, double hydrogen transfers mechanisms are considered to be much less probable than the direct hydrogen abstraction mechanism with the mechanism from the IM_AM5 complex being the most unlikely due to the high energy barrier. As a result, the double hydrogen transfer mechanism has not been involved in the HCOOH-catalyzed reaction below. Furthermore, the calculated rate ratio for $\nu_{\text{R_AM1}}/\nu_{\text{R_AM2b}}$ reveals that Channel R_AM1 is more important than that of Channel R_AM2 with the ratio of $\nu_{\text{R_AM1}}/\nu_{\text{R_AM2b}}$ is 3.95–4.01 between 280 and 320 K (Table 1).

3.3 Mechanism and kinetic for HCOOH-assisted reaction

The potential energy surfaces of the reaction channels in the presence of HCOOH for $\text{H}_2\text{O}_2 + \text{H}_2\text{O}$ formations occurring through Channels R_FA1 and R_FA2 have been displayed in Fig. 3. As for Channel R_FA1 starting from $\text{H}_2\text{O}_2 \cdots \text{HCOOH} + \text{HO}$ reactants, the route begins with the formation of the complex IM_FA1. Complex IM_FA1 forms a hydrogen-bonded configuration with a binding energy of 5.9 kcal mol⁻¹ as compared to $\text{H}_2\text{O}_2 \cdots \text{HCOOH} + \text{HO}$ reactants. The structure of IM_FA1 resembles that of $\text{H}_2\text{O}_2 \cdots \text{HCOOH}$ complex with additional two hydrogen bonds (H3 \cdots O5, 1.98 Å; O1 \cdots H4, 1.99 Å) formed between HO and $\text{H}_2\text{O}_2 \cdots \text{HCOOH}$ complex. Starting from IM_FA1 complex, the O atom of HO radical directly abstracts the H4 of H_2O_2 moiety in $\text{H}_2\text{O}_2 \cdots \text{HCOOH}$ complex, overcoming transition state TS_FA1 with an energy of 0.6 kcal mol⁻¹ with respect to $\text{H}_2\text{O}_2 \cdots \text{HCOOH} + \text{HO}$ reactants. The barrier height of Channel R_FA1 is 6.5 kcal mol⁻¹, which is lower by 7.6 kcal mol⁻¹ than the similar route in the absence of a catalyst. Meanwhile, the computed free energy barrier (ΔG , 298 K) is reduced to 7.2 kcal mol⁻¹ from 14.1 kcal mol⁻¹ in the bare $\text{H}_2\text{O}_2 + \text{HO}$ reaction. This indicates that HCOOH in Channel R_FA1 plays a positive catalytic role in the $\text{H}_2\text{O}_2 + \text{HO} \rightarrow \text{HO}_2 + \text{H}_2\text{O}$ reaction by reducing the energy barrier.

Because of relative energy, Channel R_FA2 occurring through the $\text{H}_2\text{O}_2 \cdots \text{HCOOH} + \text{HO}$ reactants is more favorable than that starting from $\text{HO} \cdots \text{HCOOH} + \text{H}_2\text{O}_2$ reactants. Given the relative concentration, the concentration of binary complex of $\text{H}_2\text{O}_2 \cdots \text{HCOOH}$ (2.10 molecules per cm³) is much higher than that of the binary complex of $\text{HO} \cdots \text{HCOOH}$ (4.17×10^{-5} molecules per cm³). However, as listed in Table 2, the ratio

($\nu_{\text{R_FA2a}}/\nu_{\text{R_FA2b}}$) between $\text{H}_2\text{O}_2 \cdots \text{HCOOH} + \text{HO}$ (Path R_FA2a) and $\text{HO} \cdots \text{HCOOH} + \text{H}_2\text{O}_2$ reaction (Path R_FA2b) in Channel R_FA2 is 0.02–0.03 between 280 and 320 K. The above facts reveal that for Channel R_FA2, the interaction between $\text{HO} \cdots \text{HCOOH} + \text{H}_2\text{O}_2$ would be more favorable than the action *via* $\text{H}_2\text{O}_2 \cdots \text{HCOOH} + \text{HO}$ route. As for Path R_FA2b, beginning with the $\text{HO} \cdots \text{HCOOH} + \text{H}_2\text{O}_2$ reactants, the reaction involves the formation of pre-reactive complex IM_FA3 with the binding energy of 11.3 kcal mol⁻¹ as compared to $\text{HO} \cdots \text{HCOOH} + \text{H}_2\text{O}_2$ reactants. In the viewpoint of geometrical structure, IM_FA3 shows a nine-membered ring with three hydrogen bonds (H3 \cdots O5, 1.84 Å; O4 \cdots H5, 1.79 Å; O2 \cdots H1, 1.75 Å) involved. After complex IM_FA3, Path R_FA2 occurs through transition state TS_FA3 where the O atom of HO radical abstracts the H atom of H_2O_2 followed by the elongation of the H5 \cdots O4 and H1 \cdots O2 bonds respectively by 0.09 Å and 0.11 Å. TS_FA3, as illustrated in Fig. 3, has a computed energy barrier of 8.9 kcal mol⁻¹ relative to complex IM_FA3, lying at 7.3 kcal mol⁻¹ below the separate reactants of $\text{H}_2\text{O}_2 + \text{HO} + \text{HCOOH}$. This barrier height is much lower than the $\text{H}_2\text{O}_2 + \text{HO} \rightarrow \text{HO}_2 + \text{H}_2\text{O}$ reaction, whose energy barrier is determined to be 14.1 kcal mol⁻¹. Similarity, the computed free energy barrier (ΔG , 298 K) is reduced to 8.9 kcal mol⁻¹ from 14.1 kcal mol⁻¹ in the bare $\text{H}_2\text{O}_2 + \text{HO}$ reaction. This indicates that HCOOH in Channel R_FA2 also plays a positive catalytic role in reducing the energy barrier of the $\text{H}_2\text{O}_2 + \text{HO} \rightarrow \text{HO}_2 + \text{H}_2\text{O}$ reaction.

As a result of the above, HCOOH-assisted $\text{H}_2\text{O}_2 + \text{HO} \rightarrow \text{HO}_2 + \text{H}_2\text{O}$ reaction mainly occurs through $\text{H}_2\text{O}_2 \cdots \text{HCOOH} + \text{HO}$ reaction (Path R_FA1) and $\text{HO} \cdots \text{HCOOH} + \text{H}_2\text{O}_2$ reaction (Path R_FA2b) by one-step route. Moreover, one-step route occurring through $\text{HO} \cdots \text{HCOOH} + \text{H}_2\text{O}_2$ reaction is more competitive than $\text{H}_2\text{O}_2 \cdots \text{HCOOH} + \text{HO}$ reaction with the ratio of $\nu_{\text{R_FA1}}/\nu_{\text{R_FA2b}}$ is 5.24–3.30 between 280 and 320 K (Table 2).

3.4 Relative impact of NH_3 and HCOOH in troposphere

From the mechanism and kinetic discussed above, X-assisted $\text{H}_2\text{O}_2 + \text{HO} \rightarrow \text{HO}_2 + \text{H}_2\text{O}$ reaction mainly proceeds through the $\text{H}_2\text{O}_2 \cdots \text{X} + \text{HO}$ reaction by one-step mechanism. Here, the relative rates for NH_3 and HCOOH to H_2O have been calculated to get a realistic diagram of the relative impact of the NH_3 and HCOOH in the troposphere. To achieve this aim, one-step reaction mechanism of $\text{H}_2\text{O}_2 + \text{HO} \rightarrow \text{HO}_2 + \text{H}_2\text{O}$ reaction assisted by H_2O at the CCSD(T)-F12a/cc-pVDZ-F12//M06-2X/aug-cc-pVTZ level has been shown in Fig. S1,[†] while its rate



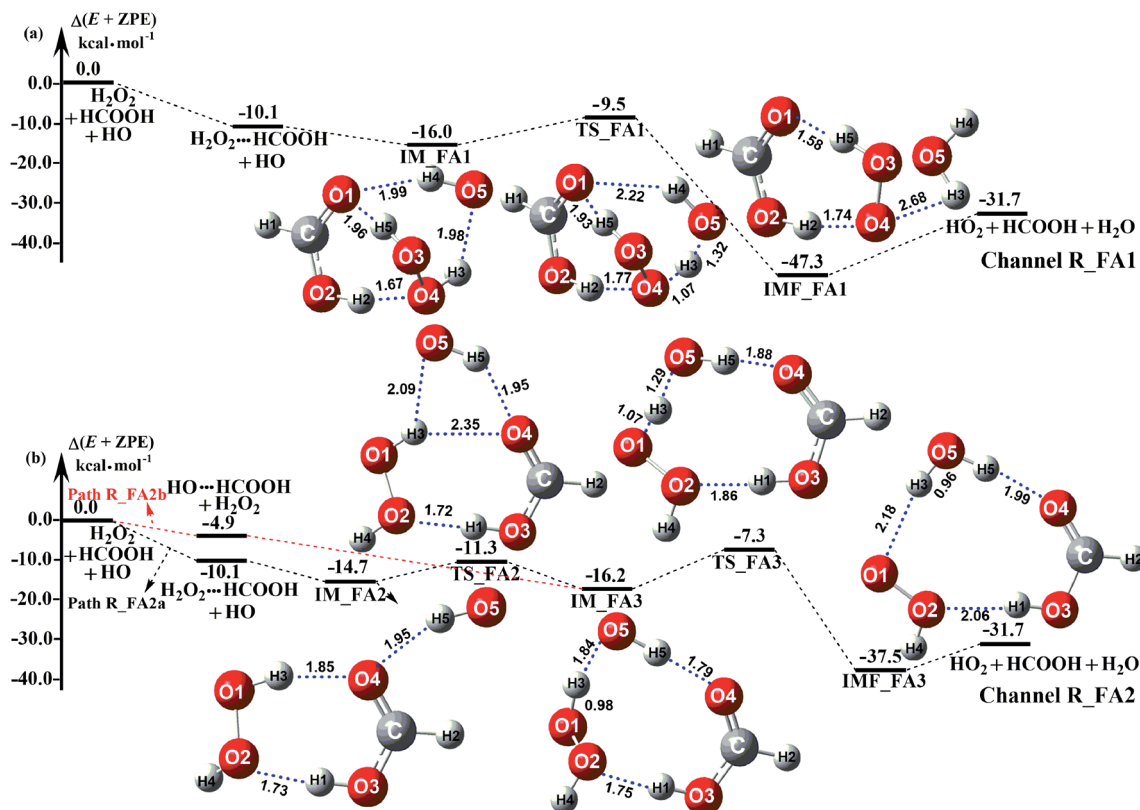


Fig. 3 Schematic potential energy diagrams for favorable channels of HCOOH catalyzed $\text{H}_2\text{O}_2 + \text{HO} \rightarrow \text{HO}_2 + \text{H}_2\text{O}$ reaction at the CCSD(T)-F12a/cc-pVDZ-F12//M06-2X/aug-cc-pVTZ level.

coefficient within the temperature range of 213–320 K is listed in Table S6.† Thus, the relative rate for NH_3 to H_2O as well as the relative rate for HCOOH as compared to H_2O is respectively given in eqn (12) and (13).

$$\frac{\nu_{\text{R_AM}}}{\nu_{\text{R_WM}}} = \frac{K_{\text{eq1a}} \times k_{\text{R_AM1}} \times [\text{H}_2\text{O}_2] \times [\text{NH}_3] \times [\text{HO}]}{K_{\text{eq1f}} \times k_{\text{R_WM}} \times [\text{H}_2\text{O}_2] \times [\text{H}_2\text{O}] \times [\text{HO}]}$$

$$= \frac{K_{\text{eq1a}} \times k_{\text{R_AM1}} \times [\text{NH}_3]}{K_{\text{eq1f}} \times k_{\text{R_WM}} \times [\text{H}_2\text{O}]}$$

$$\frac{\nu_{\text{R_FA}}}{\nu_{\text{R_WM}}} = \frac{K_{\text{eq1d}} \times k_{\text{R_FA1}} \times [\text{H}_2\text{O}_2] \times [\text{HCOOH}] \times [\text{HO}]}{K_{\text{eq1f}} \times k_{\text{R_WM}} \times [\text{H}_2\text{O}_2] \times [\text{H}_2\text{O}] \times [\text{HO}]}$$

$$= \frac{K_{\text{eq1d}} \times k_{\text{R_FA1}} \times [\text{HCOOH}]}{K_{\text{eq1f}} \times k_{\text{R_WM}} \times [\text{H}_2\text{O}]}$$

where K_{eq1a} , K_{eq1d} , and K_{eq1f} respectively denote the equilibrium constant for the formation of $\text{H}_2\text{O}_2 \cdots \text{NH}_3$, $\text{H}_2\text{O}_2 \cdots \text{HCOOH}$ and $\text{H}_2\text{O}_2 \cdots \text{H}_2\text{O}$; $k_{\text{R_AM1}}$, $k_{\text{R_FA1}}$ and $k_{\text{R_WM}}$ respectively denote the bimolecular rate coefficient for the favorable one-step mechanism in $\text{H}_2\text{O}_2 + \text{HO} \rightarrow \text{HO}_2 + \text{H}_2\text{O}$ reaction assisted by NH_3 , HCOOH and H_2O . $[\text{NH}_3]$, $[\text{HCOOH}]$ and $[\text{H}_2\text{O}]$ are the concentration of NH_3 , HCOOH and H_2O , which was obtained from previous report values.^{55,64,65,70,75}

The relative rates for $\nu_{\text{R_AM1}}/\nu_{\text{R_WM}}$ and $\nu_{\text{R_FA1}}/\nu_{\text{R_WM}}$ within the temperature range of 280–320 K are given in Table 3. As seen in Table 3, when the concentrations of H_2O at 100% (2.60×10^{17} molecule per cm^3 to 2.30×10^{18} molecule per cm^3)⁷⁶ RH and NH_3 at 10 ppbv (2.60×10^{11} molecule per cm^3 to 2.30×10^{11} molecule per cm^3),^{22–24} the calculated $\nu_{\text{R_AM1}}/\nu_{\text{R_WM}}$ value is below 2.47×10^{-3} to 9.40×10^{-5} within the temperature range

Table 2 The bimolecular rate coefficients (cm^3 per molecules per s) and rate ratio for HCOOH catalyzed $\text{H}_2\text{O}_2 + \text{HO} \rightarrow \text{HO}_2 + \text{H}_2\text{O}$ reaction within the temperature range of 280–320 K

T/K	$k_{\text{R_FA1}}$	$k_{\text{R_FA2a}}$	$k_{\text{R_FA2b}}$	$\nu_{\text{R_FA2a}}/\nu_{\text{R_FA2b}}$	$\nu_{\text{R_FA1}}/\nu_{\text{R_FA2b}}$
280	9.50×10^{-11}	3.95×10^{-13}	1.86×10^{-8}	0.02	5.24
290	7.32×10^{-11}	3.87×10^{-13}	1.09×10^{-8}	0.02	4.64
298	6.07×10^{-11}	3.82×10^{-13}	7.29×10^{-9}	0.03	4.19
300	5.81×10^{-11}	3.81×10^{-13}	6.64×10^{-9}	0.03	4.10
310	4.67×10^{-11}	3.78×10^{-13}	4.20×10^{-9}	0.03	3.65
320	3.83×10^{-11}	3.79×10^{-13}	2.76×10^{-9}	0.03	3.30



Table 3 The pseudo-first-order rate coefficients (cm^3 per molecules per s) for H_2O , NH_3 and HCOOH catalyzed $\text{H}_2\text{O}_2 + \text{HO} \rightarrow \text{HO}_2 + \text{H}_2\text{O}$ reaction within the temperature range of 280–320 K

T/K	$k'_t(\text{R_WM})$ (100% RH)	$k'_t(\text{R_AM1})$ (10 ppbv)	$k'_t(\text{R_AM1})$ (2900 ppbv)	$k'_t(\text{R_FA1})$ (high 10 ppbv)
280	2.13×10^{-17}	5.25×10^{-20}	1.53×10^{-17}	5.19×10^{-19}
290	3.29×10^{-17}	3.20×10^{-20}	9.35×10^{-18}	2.34×10^{-19}
298	4.63×10^{-17}	2.29×10^{-20}	6.50×10^{-18}	1.27×10^{-19}
300	5.01×10^{-17}	2.02×10^{-20}	5.99×10^{-18}	1.12×10^{-19}
310	7.54×10^{-17}	1.39×10^{-20}	3.99×10^{-18}	5.82×10^{-20}
320	1.01×10^{-16}	9.49×10^{-21}	2.76×10^{-18}	3.07×10^{-20}

T/K	$\nu_{\text{R_AM1}}(10 \text{ ppbv})/\nu_{\text{R_WM}}$ (100% RH)	$\nu_{\text{R_AM1}}(2900 \text{ ppbv})/\nu_{\text{R_WM}}$ (100% RH)	$\nu_{\text{R_FA1}}(\text{high})/\nu_{\text{R_WM}}$ (100% RH)
280	2.47×10^{-3}	0.72	2.44×10^{-2}
290	9.73×10^{-4}	0.28	7.13×10^{-3}
298	4.94×10^{-4}	0.14	2.75×10^{-3}
300	4.04×10^{-4}	0.12	2.23×10^{-3}
310	1.84×10^{-4}	5.29×10^{-2}	7.72×10^{-4}
320	9.40×10^{-5}	2.74×10^{-2}	3.05×10^{-4}

of 280–320 K. Moreover, when the concentration of NH_3 at 2900 ppbv (7.60×10^{13} molecule per cm^3 to 6.70×10^{13} molecule per cm^3),²⁵ the calculated $\nu_{\text{R_AM1}}/\nu_{\text{R_WM}}$ is still below 0.72–2.74 $\times 10^{-2}$. This reveals that the $\text{H}_2\text{O}_2 + \text{HO} \rightarrow \text{HO}_2 + \text{H}_2\text{O}$ reaction with NH_3 cannot compete with the reaction in the presence of H_2O . Similarly, when the concentration of HCOOH at 2.60×10^{11} molecule per cm^3 to 2.30×10^{11} molecule per cm^3 ,⁷⁷ the calculated $\nu_{\text{R_FA1}}/\nu_{\text{R_WM}}$ value is 2.44×10^{-2} to 3.05×10^{-4} within the temperature range of 280–320 K, indicating that the $\text{H}_2\text{O}_2 + \text{HO} \rightarrow \text{HO}_2 + \text{H}_2\text{O}$ reaction with HCOOH also cannot compete with the corresponding reaction in the presence of H_2O .

4. Summary and conclusions

The effect of catalyst X (X = NH_3 and HCOOH) on the $\text{H}_2\text{O}_2 + \text{HO} \rightarrow \text{HO}_2 + \text{H}_2\text{O}$ reaction was investigated by using quantum chemical calculations and canonical variational transition state theory with small curvature tunneling correction. Two kinds of acid–base catalyzed mechanism, namely one-step route and stepwise processes, were found in the reaction assisted by catalyst X. As for the one-step route, the reaction proceeded through similar direct hydrogen abstraction with the reaction without catalyst X. We found one-step mechanism that is promoted by a low energy barrier, was respectively predicted to take place at a bimolecular rate coefficient of 9.95×10^{-11} cm^3 per molecule per s (NH_3 -assisted reaction) and 6.07×10^{-11} cm^3 per molecule per s (HCOOH -assisted reaction) at 298 K, and is very closed to the rate coefficient for the reaction without catalyst X. Stepwise processes here were explored by direct hydrogen abstraction and double hydrogen abstraction transfer mechanism, and were found to be kinetically more favorable *via* direct hydrogen abstraction. However, this hydrogen abstraction in a stepwise route is essentially less important than the hydrogen abstraction in a one-step mechanism.

Within the temperature ranging from 280 K to 320 K, the pseudo-first-order rate coefficient for one-step mechanism in the presence of NH_3 (10 ppbv) and HCOOH (10 ppbv) is only 5.25×10^{-20} to 9.49×10^{-21} cm^3 per molecule per s and 5.19×10^{-19} to 3.07×10^{-20} cm^3 per molecule per s, respectively. This was largely decreased by 3–5 and 2–4 orders of magnitude than the reaction assisted by H_2O in which the positive water effect is significant under atmospheric conditions. This catalytic difference between catalyst X and H_2O is possibly due to a much lower concentration of NH_3 and HCOOH relative to H_2O . Despite the fact that $\text{H}_2\text{O}_2 + \text{HO} \rightarrow \text{HO}_2 + \text{H}_2\text{O}$ reaction with catalyst X is not so efficient to shift the overall $\text{HO}_2 + \text{H}_2\text{O}$ formation rate, the present study provides a comprehensive model of how acidic and basic catalysts assisted the gas-phase reactions.

Conflicts of interest

The authors declare no competing financial interest.

Acknowledgements

This work was supported by the National Natural Science Foundation of China (No: 21603132), the Shaanxi Provincial Natural Science Foundation (No: 2019JM-336 and 2019JQ-880), the Shaanxi Provincial Department of Education Project (18JK0147 and 18JS022), Shanghai Science and Technology Committee (16DZ2270100).

References

- 1 T. P. Marcy, D. W. Fahey, R. S. Gao, P. J. Popp, E. C. Richard, T. L. Thompson, K. H. Rosenlof, E. A. Ray, R. J. Salawitch, C. S. Atherton, D. J. Bergmann, B. A. Ridley, A. J. Weinheimer, M. Loewenstein, E. M. Weinstock and M. J. Mahoney, *Science*, 2004, **304**, 261–265.



- 2 P. A. Ariya, R. Sander and P. J. Crutzen, *J. Geophys. Res.: Atmos.*, 2000, **105**, 17721–17738.
- 3 Y. Elshorbany, I. Barnes, K. H. Becker, J. Kleffmann and P. Wiesen, *Z. Physiol. Chem.*, 2010, **224**, 967–987.
- 4 A. Mansergas and J. M. Anglada, *ChemPhysChem*, 2007, **8**, 1534–1539.
- 5 S. A. Nizkorodov, W. W. Harper, B. W. Blackmon and D. J. Nesbitt, *J. Phys. Chem. A*, 2000, **104**, 3964–3973.
- 6 T. J. Wallington, K. W. Jucks and G. S. Tyndall, *Int. J. Chem. Kinet.*, 1998, **30**, 707–709.
- 7 E. Jiménez, T. Gierczak, H. Stark, J. B. Burkholder and A. R. Ravishankara, *J. Phys. Chem. A*, 2004, **108**, 1139–1149.
- 8 A. A. Turnipseed, G. L. Vaghjiani, T. Gierczak, J. E. Thompson and A. R. Ravishankara, *J. Chem. Phys.*, 1991, **95**, 3244–3251.
- 9 G. L. Vaghjiani and A. R. Ravishankara, *J. Chem. Phys.*, 1990, **92**, 996–1003.
- 10 G. L. Vaghjiani, A. R. Ravishankara and N. Cohen, *J. Phys. Chem.*, 1989, **93**, 7833–7837.
- 11 F. Temps and H. Gg. Wagner, *Bunsen-Ges. Phys. Chem., Ber.*, 1982, **86**, 119–125.
- 12 W. J. Marinelli and H. S. Johnston, *J. Chem. Phys.*, 1982, **77**, 1225–1234.
- 13 F. Atadinc, H. Günaydin, A. S. Özen and V. Aviyente, *Int. J. Chem. Kinet.*, 2005, **37**, 502–514.
- 14 R. R. Baldwin and R. W. Walker, *J. Chem. Soc., Faraday Trans.*, 1979, **75**, 140–154.
- 15 P. H. Wine, D. H. Semmes and A. R. Ravishankara, *J. Chem. Phys.*, 1981, **75**, 4390–4395.
- 16 A. B. Vakhtin, D. C. McCabe, A. R. Ravishankara and S. R. Leone, *J. Phys. Chem. A*, 2003, **107**, 10642–10647.
- 17 S. P. Sander, D. M. Golden, M. J. Kurylo, G. K. Moortgat, P. H. Wine, A. R. Ravishankara, C. E. Kolb, M. J. Molina, B. J. Finlayson-Pitts and R. E. Huie, *Chemical kinetics and photochemical data for use in atmospheric studies evaluation number 15*, 2006.
- 18 E. Vöhringer-Martinez, B. Hansmann, H. Hernandez-Soto, J. S. Francisco, J. Troe and B. Abel, *Science*, 2007, **315**, 497–501.
- 19 Z. K. Hong, R. D. Cook, D. F. Davidson and R. K. Hanson, *J. Phys. Chem. A*, 2010, **114**, 5718–5727.
- 20 R. J. Buszek, M. Torrent-Sucarrat, J. M. Anglada and J. S. Francisco, *J. Phys. Chem. A*, 2012, **116**, 5821–5829.
- 21 T. L. Zhang, X. G. Lan, Y. H. Zhang, R. Wang, Y. Q. Zhang, Z. Y. Qiao and N. Li, *Mol. Phys.*, 2019, **117**, 516–530.
- 22 J. J. Orlando, G. S. Tyndall and G. P. Brasseur, *Atmospheric chemistry and global change*, Oxford University Press, 1999.
- 23 V. P. Aneja, D. R. Nelson, P. A. Roelle, J. T. Walker and W. Battye, *J. Geophys. Res.: Atmos.*, 2003, **108**(D4), 4152.
- 24 J. X. Warner, Z. Wei, L. L. Strow, R. R. Dickerson and J. B. Nowak, *Atmos. Chem. Phys. Discuss.*, 2015, **15**, 35823–35856.
- 25 N. Hiranuma, S. D. Brooks, D. C. O. Thornton and B. W. Auvermann, *J. Air Waste Manage. Assoc.*, 2010, **60**, 210–218.
- 26 B. Bandyopadhyay, P. Biswas and P. Kumar, *Phys. Chem. Chem. Phys.*, 2016, **18**, 15995–16004.
- 27 B. Bandyopadhyay, P. Kumar and P. Biswas, *J. Phys. Chem. A*, 2017, **121**, 3101–3108.
- 28 T. L. Zhang, Y. Q. Zhang, M. J. Wen, Z. Tang, B. Long, X. H. Yu, C. B. Zhao and W. L. Wang, *RSC Adv.*, 2019, **9**, 21544–21556.
- 29 B. Long, X. F. Tan, Y. B. Wang, J. Li, D. S. Ren and W. J. Zhang, *ChemistrySelect*, 2016, **1**, 1421–1430.
- 30 M. L. Wei, X. F. Tan, Z. W. Long and B. Long, *RSC Adv.*, 2017, **7**, 56211–56219.
- 31 S. Mallick, S. Sarkar, P. Kumar and B. Bandyopadhyay, *J. Phys. Chem. A*, 2017, **122**, 350–363.
- 32 S. Ghoshal and M. K. Hazra, *RSC Adv.*, 2015, **5**, 17623–17635.
- 33 R. J. Buszek, A. Sinha and J. S. Francisco, *J. Am. Chem. Soc.*, 2011, **133**, 2013–2015.
- 34 M. K. Hazra and T. Chakraborty, *J. Phys. Chem. A*, 2006, **110**, 9130–9136.
- 35 G. D. Silva, *Angew. Chem., Int. Ed.*, 2010, **49**, 7523–7525.
- 36 M. K. Hazra and T. Chakraborty, *J. Phys. Chem. A*, 2005, **109**, 7621–7625.
- 37 B. Long, Z. Long, Y. Wang, X. Tan, Y. Han, C. Long, S. Qin and W. Zhang, *ChemPhysChem*, 2012, **13**, 323–329.
- 38 M. J. Frisch, G. Trucks, J. A. Pople, *et al.*, *Gaussian 09, Revision A.01*, Gaussian Inc, Pittsburgh, PA, 2009.
- 39 K. Fukui, *Acc. Chem. Res.*, 1981, **14**, 363–368.
- 40 C. Gonzalez and H. B. Schlegel, *J. Chem. Phys.*, 1989, **90**, 2154–2161.
- 41 M. page and J. W. McIver Jr, *J. Chem. Phys.*, 1988, **88**, 922–935.
- 42 F. Neese, *Wiley Interdiscip. Rev.: Comput. Mol. Sci.*, 2012, **2**, 73–78.
- 43 N. Bork, J. Elm, T. Olenius and H. Vehkamäki, *Atmos. Chem. Phys.*, 2014, **14**, 12023–12030.
- 44 N. Myllys, J. Elm, R. Halonen, T. Kurtén and H. Vehkamäki, *J. Phys. Chem. A*, 2016, **120**, 621–630.
- 45 J. Elm and K. Kristensen, *Phys. Chem. Chem. Phys.*, 2017, **19**, 1122–1133.
- 46 D. Kashinski, G. Chase, R. Nelson, O. Di Nallo, A. Scales, D. VanderLey and E. F. C. Byrd, *J. Phys. Chem. A*, 2017, **121**, 2265–2273.
- 47 B. Chan and L. Radom, *J. Chem. Theory Comput.*, 2015, **11**, 2109–2119.
- 48 Z. Rolik, L. Szegedy, I. Ladjánszki, B. Ladóczki and M. Kállay, *J. Chem. Phys.*, 2013, **139**, 094105.
- 49 M. Kállay, Z. Rolik, I. Ladjánszki, L. Szegedy, B. Ladóczki, J. Csontos and B. Kornis, *MRCC, A Quantum Chemical Program Suite*, 2015, see www.mrcc.hu, 2019.
- 50 B. Long, J. L. Bao and D. G. Truhlar, Unimolecular reaction of acetone oxide and its reaction with water in the atmosphere, *Proc. Natl. Acad. Sci. U. S. A.*, 2018, **115**, 6135–6140.
- 51 B. Long, J. L. Bao and D. G. Truhlar, *Phys. Chem. Chem. Phys.*, 2017, **19**, 8091–8100.
- 52 B. Long, J. L. Bao and D. G. Truhlar, *J. Am. Chem. Soc.*, 2016, **138**, 14409–14422.
- 53 B. Long, J. L. Bao and D. G. Truhlar, *J. Am. Chem. Soc.*, 2018, **141**, 611–617.



- 54 Y. Chuang, J. Corchado, P. Fast, J. Villà, E. Coitino, W. Hu, Y. Liu, G. Lynch, K. Nguyen and C. Jackels, *POLYRATE, Version 8.2*, Department of Chemistry and Supercomputer Institute, University of Minnesota, Minnesota, CP, 1999.
- 55 J. L. Bao and D. G. Truhlar, *Chem. Soc. Rev.*, 2017, **46**, 7548–7596.
- 56 B. C. Garrett and D. G. Truhlar, *J. Chem. Phys.*, 1979, **70**, 1593–1598.
- 57 B. C. Garrett and D. G. Truhlar, *J. Am. Chem. Soc.*, 1979, **101**, 4534–4548.
- 58 B. C. Garrett, D. G. Truhlar, R. S. Grev and A. W. Magnuson, *J. Phys. Chem.*, 1980, **84**, 1730–1748.
- 59 Y. P. Liu, G. C. Lynch, T. N. Truong, D. H. Lu, D. G. Truhlar and B. C. Garrett, *J. Am. Chem. Soc.*, 1993, **115**, 2408–2415.
- 60 D. H. Lu, T. N. Truong, V. S. Melissas, G. C. Lynch, Y. P. Liu, B. C. Garrett, R. Steckler, A. D. Isaacson, S. N. Rai, G. C. Hancock, J. G. Lauderdale, T. Joseph and D. G. Truhlar, *Comput. Phys. Commun.*, 1992, **71**, 235–262.
- 61 T. L. Zhang, R. Wang, H. Chen, S. T. Min, Z. Y. Wang, C. B. Zhao, Q. Xu, L. X. Jin, W. L. Wang and Z. Q. Wang, *Phys. Chem. Chem. Phys.*, 2015, **17**, 15046–15055.
- 62 T. L. Zhang, X. G. Lan, Z. Y. Qiao, R. Wang, X. H. Yu, Q. Xu, Z. Y. Wang, L. X. Jin and Z. Q. Wang, *Phys. Chem. Chem. Phys.*, 2018, **20**, 8152–8165.
- 63 C. Iuga, J. R. Alvarez-Idaboy and A. Vivier-Bunge, *Theor. Chem. Acc.*, 2011, **129**, 209–217.
- 64 M. A. Ali, M. Balaganesh and K. C. Lin, *Phys. Chem. Chem. Phys.*, 2018, **20**, 4297–4307.
- 65 R. Wang, Q. Y. Yao, M. J. Wen, S. B. Tian, Y. Wang, Z. Y. Wang, X. H. Yu, X. Z. Shao and L. Chen, *RSC Adv.*, 2019, **9**, 16195–16207.
- 66 M. A. Ali, M. Balaganesh and S. Jang, *Atmos. Environ.*, 2019, **207**, 82–92.
- 67 Z. G. Dong, F. Xu and B. Long, *Comput. Theor. Chem.*, 2018, **1140**, 7–13.
- 68 F. Y. Liu, X. F. Tan, Z. W. Long, B. Long and W. J. Zhang, *RSC Adv.*, 2015, **5**, 32941–32949.
- 69 X. F. Tan, B. Long, D. S. Ren, W. J. Zhang, Z. W. Long and E. Mitchell, *Phys. Chem. Chem. Phys.*, 2018, **20**, 7701–7709.
- 70 S. Sarkar, B. K. Oram and B. Bandyopadhyay, *J. Phys. Chem. A*, 2019, **123**, 3131–3141.
- 71 X. Chen, Y. F. Zhao, L. S. Wang and J. Li, *Comput. Theor. Chem.*, 2017, **1107**, 57–65.
- 72 Y. F. Zhao, X. Chen and J. Li, *Nano Res.*, 2017, **10**, 3407–3420.
- 73 T. L. Zhang, C. Yang, X. K. Feng, J. X. Kang, L. Song, Y. S. Lu, Z. Y. Wang, Q. Xu, W. L. Wang and Z. Q. Wang, *Phys. Chem. Chem. Phys.*, 2016, **18**, 17414–17427.
- 74 T. L. Zhang, K. Wang, Z. Y. Qiao, Y. Q. Zhang, L. Geng, R. Wang, Z. Y. Wang, C. B. Zhao and L. X. Jin, *RSC Adv.*, 2018, **8**, 37105–37116.
- 75 B. Du and W. C. Zhang, *J. Phys. Chem. A*, 2013, **117**, 6883–6892.
- 76 S. Sarkar, S. Mallick, D. Kaushik, P. Kumar and B. Bandyopadhyay, *Phys. Chem. Chem. Phys.*, 2017, **19**, 27848–27858.
- 77 T. Stavrou, J. Müller, J. Peeters, A. Razavi, L. Clarisse, C. Clerbaux, P. F. Coheur, D. Hurtmans, M. De Mazière, C. Vigouroux, N. M. Deutscher, D. W. T. Griffith, N. Jones and C. Paton-Walsh, *Nat. Geosci.*, 2012, **5**, 26–30.

